Spin and charge dynamics of stripes in doped Mott insulators.

F.F. Assaad[1,2], V. Rousseau[3], F. Hebert[4], M. Feldbacher[1] and G. G. Batrouni[3]
1. Institut für Theoretische Physik III, Universität Stuttgart, Pfaffenwaldring 58, D-70550 Stuttgart, Germany.
2. Max Planck institute for solid state research, Heisenbergstr. 1, D-70569, Stuttgart, Germany
3. Institut Non-Linéaire de Nice, Université de Nice-Sophia Antipolis, 1361 route des Lucioles, 06560 Valbonne, France
4. Theoretische Physik, Universität des Saarlandes, 66041 Saarbrücken, Germany

We study spin and charge dynamics of stripes in doped Mott insulators by considering a two-dimensional Hubbard model with N fermion flavors. For $N = 2$ we recover the normal one-band model while for $N \to \infty$ a spin density wave mean-field solution. For all band fillings, lattice topologies and $N = 4n$ the model may be solved by means of Monte Carlo methods without encountering the sign problem. At $N = 4$ and in the vicinity of the Mott insulator, the single particle density of states shows a gap. Within this gap and on rectangular topologies of sizes up to 30×12 we find gapless spin collective modes centered around $\vec{q} = (\pi \pm \epsilon_x, \pi \pm \epsilon_y)$ as well as charge modes centered around $\vec{q} = (\pm 2\epsilon_x, \pm 2\epsilon_y)$, $\vec{q} = (\pm\epsilon_x, \pm\epsilon_y)$ and $\vec{q} = (0, 0)$. $\epsilon_{x,y}$ depends on the lattice topology and doping.

PACS numbers: 71.27.+a, 71.10.-w, 71.10.Fd

The understanding of the interplay between spin and charge degrees of freedom in doped two-dimensional Mott insulators remains a challenging issue. On the analytical front, it is straightforward to apply the Hartree-Fock (HF) approximation but the difficulty lies in taking quantum fluctuations into account. On the other hand numerical methods take into account fluctuations but are limited to small clusters due to the size of the Hilbert space, for exact diagonalization, or due to the minus sign problem inherent to quantum Monte Carlo (QMC) methods. In this letter, we introduce a QMC method which lies between HF and full quantum fluctuations and apply it to the doped two dimensional Hubbard model. Since the $N-$flavor model we consider breaks $SU(N)$ spin symmetry it favors spin states. In particular in the vicinity of the Mott insulator (MI) we find a stripe phase experimentally observed in cuprates and nickelates [1, 2]. Our simulations reveal the dynamics of this phase.

Our starting point is the Hamiltonian:

$$H = -t \sum_{(\vec{i},\vec{j})} \mathbf{c}_{\vec{i}}^{\dagger} \mathbf{c}_{\vec{j}} - \frac{U}{N} \sum_{\vec{i}} \left(\mathbf{c}_{\vec{i}}^{\dagger} \lambda \mathbf{c}_{\vec{i}} \right)^2 \qquad (1)$$

where $\vec{i}$ labels the sites of a square lattice and the first sum runs over nearest neighbors. The spinors $\mathbf{c}_{\vec{i}}^{\dagger} = \left(c_{\vec{i},1}^{\dagger} \cdots c_{\vec{i},N}^{\dagger} \right)$ correspond to fermions with N flavors. For even values of N, $\lambda_{\alpha,\gamma} = \delta_{\alpha,\gamma} f(\alpha)$ with $f(\alpha) = 1$ for $\alpha \leq N/2$ and -1 otherwise. At $N = 2$ the model reduces to the standard $SU(2)$-spin invariant Hubbard model since the interaction is the square of the magnetization. Away from $N = 2$ the model has an $SU(N/2) \otimes SU(N/2)$ symmetry which becomes clear when writing the Hamiltonian in terms of the spinors: $\left(c_{\vec{i},1}^{\dagger} \cdots c_{\vec{i},N/2}^{\dagger} \right)$ and $\left(c_{\vec{i},N/2+1}^{\dagger} \cdots c_{\vec{i},N}^{\dagger} \right)$. As $N \to \infty$ the exact solution of the model reduces to a spin density wave mean-field approximation.

The central observation is that at $N = 4n$ the minus sign problem in QMC approach is never present regardless of the lattice topology and band-filling. To illustrate this and to keep the notation simple we consider the finite temperature auxiliary field QMC approach. After the usual decoupling of the interaction term with a Hubbard-Stratonovich transformation, the partition function becomes $Z = \int \mathcal{D}\phi e^{-NS(\phi)}$, where

$$\begin{aligned} S(\phi) &= U \int_0^{\beta} \mathrm{d}\tau \frac{\sum_{\vec{i}} \Phi_{\vec{i}}^2(\tau)}{4} - \frac{1}{2} \ln \mathrm{Tr} \left[T e^{-\int_0^{\beta} \mathrm{d}\tau H(\tau)} \right] \qquad (2) \\ H(\tau) &= -t \sum_{(\vec{i},\vec{j}),\sigma=\pm 1} c_{\vec{i},\sigma}^{\dagger} c_{\vec{j},\sigma} - U \sum_i \Phi_{\vec{i}}(\tau) \left(n_{\vec{i},+} - n_{\vec{i},-} \right). \end{aligned}$$

Here T corresponds to time ordering and in terms of our original fermions we can identify: $c_{\vec{i},+} = c_{\vec{i},1}$ and $c_{\vec{i},-} = c_{\vec{i},N/2+1}$. As $N \to \infty$ the integral over the fields ϕ is dominated by the saddle point configuration, ϕ^* satisfying $\partial S(\phi)/\partial\phi|_{\phi=\phi^*} = 0$. A time independent solution is $\Phi_i^{\star} = \langle n_{\vec{i},+} - n_{\vec{i},-} \rangle$ where the expectation value is taken with respect to the Hamiltonian in Eq. 2. This is precisely the set of self-consistent equations obtained from the mean-field decoupling: $n_{i,+} - n_{i,-} = \Phi_i^{\star} + [(n_{i,+} - n_{i,-}) - \Phi_i^{\star}]$ for the Hamiltonian of Eq. 1 at $N = 2$.

Since $\mathrm{Tr} \left[T e^{-\int_0^{\beta} \mathrm{d}\tau H(\tau)} \right]$ is a real number for $U > 0$, it follows that $NS(\Phi)$ is real for $N = 4n$. This observation allows us to interpret $e^{-NS(\Phi)}$ as a probability distribution which we sample with Monte Carlo methods. Hence for $N = 4n$ the sign problem never occurs regardless of doping and lattice topology. For the simulations, we have used the related projector auxiliary field QMC algorithm which is better suited for the study of ground state properties [3]. Dynamical information is obtained by using the Maximum Entropy method [4]. The details of the approach will be discussed elsewhere.

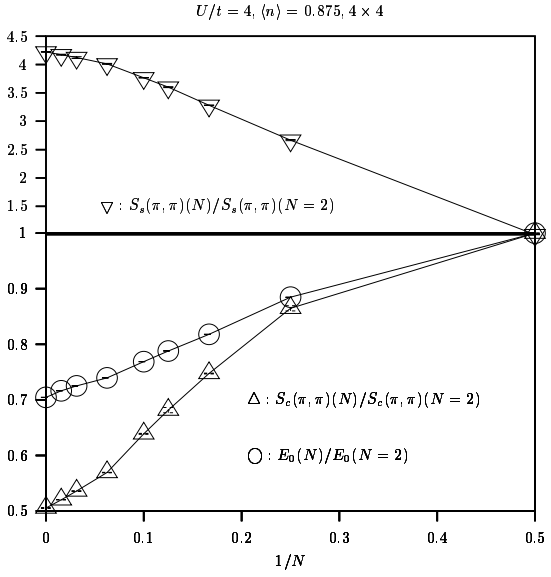

FIG. 1: Ground state energy as well as spin and charge structure factors at $\vec{q} = (\pi, \pi)$. The data points at $N = 2$ stem from exact diagonalization studies [6].

To test and interpret our approach, we show in Fig. 1 the static spin and charge structure factors,

$$S_s^c(q) = \sum_{\vec{r}} e^{i\vec{r}\vec{q}} \langle (n_{0,+} \pm n_{0,-})(n_{r,+} \pm n_{r,-})\rangle, \quad (3)$$

as well as the ground state energy as a function of $1/N$ on a 4×4 lattice, $U/t = 4$ and two holes doped away from half-filling. The electron density is defined as: $\langle n\rangle = \frac{1}{V}\sum_{\vec{i}} \langle n_{\vec{i},+} + n_{\vec{i},-}\rangle$ where V is the number unit cells $\vec{i}$. In spite of sign problems for $N \neq 4n$, the QMC data interpolate between the mean-field solution at $N = \infty$ and the exact diagonalization results at $N = 2$. In the context of the large-N approach [5] Gaussian fluctuations correspond to $1/N$ corrections. Fig. 1 shows that this approximation is valid till $N \simeq 16$. Hence, $N = 4$ is far beyond this approximation. In particular in the strong coupling limit, the model at $N = 4$ generates a magnetic scale proportional to t^2/U; a phenomena which is beyond Gaussian fluctuations around a weak coupling saddle point. Since we are solving the model *exactly* for a given value of N lattice symmetries, which are broken at the HF level, are restored in the QMC calculations.

We use the method to investigate the metallic phase in the vicinity of the MI. To maximize quantum fluctuations, we concentrate on the $N = 4$ case. In the vicinity of the MI state, the relevant length scale is set by the inverse doping $1/\delta$. To achieve this length scale at least along one lattice direction, we will consider rectangular topologies of width ranging up to 12 lattice constants. We adopt periodic boundary conditions in both lattice directions.

We start with single particle excitations. The density of states $N(\omega)$ as a function of doping is plotted in Fig.

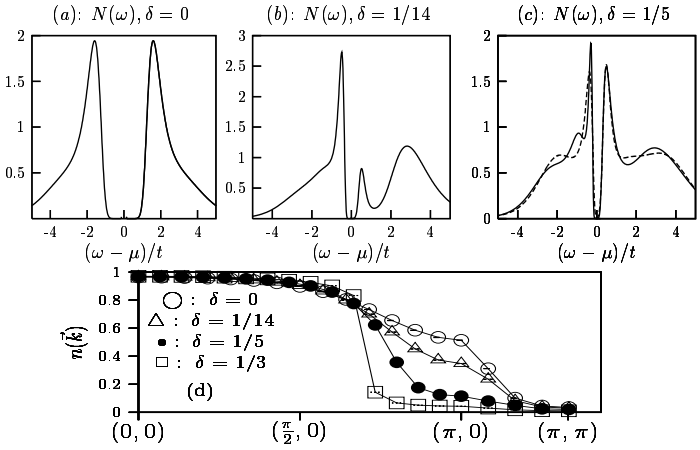

FIG. 2: Density of states as a function of doping. The lattice sizes are: (a)-(b) 28×8, (c) 30×8 (solid line) 30×12 dashed line. (d) Single particle occupation number. We have set $U/t = 3$, $N = 4$ and $T = 0$.

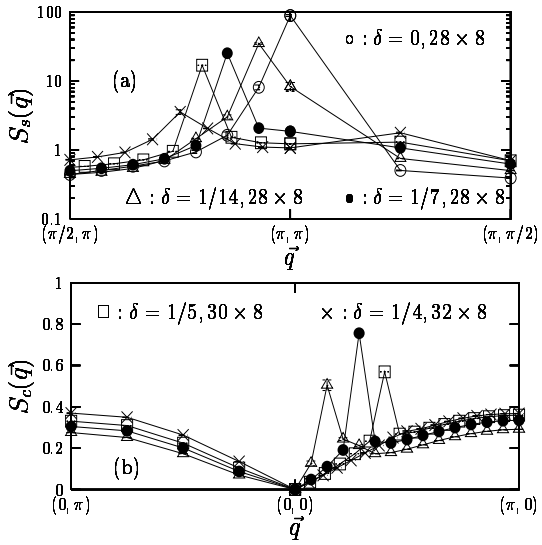

FIG. 3: Spin (a) and charge (b) structure factors as a function of doping at $U/t = 3$.

2 for various fillings. At $U/t = 3$, $N = 4$ and half-filling, we see a Mott gap of approximately $2t$ (Fig. 2a). Upon doping, the chemical potential shifts into the lower Hubbard band and spectral weight is transfered from the upper Hubbard band to generate low a energy feature [7]. In particular, at $\delta = 1/14$ remnants of the upper Hubbard band ($\approx 2t$ away from μ) are seen and a low energy feature is detectable. The data of Fig. 2 also show the presence of a small quasiparticle gap at finite dopings. This is confirmed by the single particle occupation number $n(\vec{k})$ which shows a smooth behavior up to $\delta = 1/5$.

The origin of the quasiparticle gap lies in magnetic fluc-

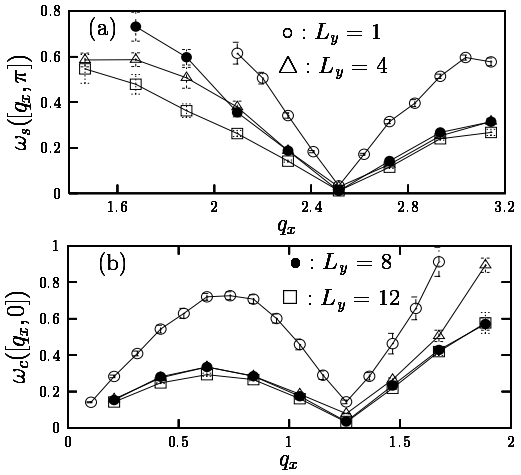

FIG. 4: Leading edge of the spin (a) and charge (b) dynamical structure factor as as function of width L_y at $U/t = 3$, $\delta = 0.2$, $T = 0$ and $N = 4$. We consider $L_x = 60$ for $L_y = 1$ and $L_x = 30$ otherwise. Note that at $L_y = 1$ the second component of the wave vector has no meaning.

tuations which remain substantial away from half-filling. Fig. 3 shows the spin and charge structure factors for several dopings δ on rectangles of width $L_y = 8$. For those topologies, the dominant features are along the $(1, 0)$ direction. In particular we see a peak in the spin structure factor at $\vec{Q}_s = (\pi - \epsilon_x, \pi)$ accompanied by one in the charge structure factor at $\vec{Q}_c = (2\epsilon_x, 0)$ with $\epsilon_x = \pi\delta$. Transforming the data in real space yields the stripe caricature: rivers of holes along the y-direction separated by $1/\delta$ lattice constants in the x-direction. Across each river of holes, there is a π-phase shift in the spin structure with respect to the antiferromagnetic ordering. Similar features are seen in one dimension (1D) where our simulations at $N = 4$ show dominant cusps in the charge (spin) structures factors at $4k_f \equiv 2\pi\delta$ ($2k_f \equiv \pi - \pi\delta$) [8]. In 1D we checked successfully for power law decay of the $2k_f$ spin and $4k_f$ charge correlation function at $N = 4$. On fixed width topologies one would equally expect power law decay of the correlation functions. We were however unable to confirm this numerically due to limitations on lattice sizes.

To study the dynamical properties of the striped phase, we compute the imaginary time displaced spin and charge correlation functions : $S_{c/s}(\vec{q}, \tau)$. By fitting the tail $S_{c/s}(\vec{q}, \tau)$ to a single exponential, we obtain the leading edge of the charge and spin excitation spectra: $\omega_{c/s}(\vec{q})$. Irrespective of lattice width the overall features of the QMC data of Fig. 4 suggest gapless spin [charge] excitations with linear dispersions around $\vec{Q}_s$ [$\vec{Q}_c$ and $(0, 0)$]. The data equally show other features. (i) At $L_y = 8, 12$, the spin and charge excitations lie below the particle-hole continuum which from the single particle density of states (see Fig. 2(c)) lies at a threshold energy $2\Delta_{qp} \approx 0.5t$. (ii) The continuity equation, $\frac{d}{dt} n(\vec{x}, t) + \vec{\nabla} \cdot \vec{J}(\vec{x}, t) = 0$ yields an identity between the dynamical charge structure factor and the real part of the optical conductivity $\sigma'(\vec{q}, \omega)$: $\omega S_c(\vec{q}, \omega)/q_x^2 \equiv \sigma'_{x,x}(\vec{q}, \omega)$. Thus long wave length charge modes carry current so that we have a metallic state. Direct QMC evaluation of the conductivity confirms this.

It is tempting to try to understand the above excitation spectrum for our finite width lattices as evolving from 1D physics [8, 9]. Here we would however like to discuss two other possibilities in terms of Goldstone modes. (i) As mentioned previously, the model at $N = 4$ has an $SU(2) \otimes SU(2)$ symmetry and one may be tempted to interpret the low lying spin and charge features in terms of Goldstone modes associated with the breaking of this continuous symmetry. Our calculations do not support this point view since those modes remain disordered. (ii) To interpret the data in terms of the dynamics of spin and charge density waves [10, 11], we have to argue that the pinning of those modes due to the lattice is small. To do so, we carry out a HF calculation with order parameters: $\langle n_{\vec{r},+} - n_{\vec{r},-} \rangle = \Delta_s \cos(\vec{Q}_s \vec{r} + \phi_s)$ and $\langle n_{\vec{r},+} + n_{\vec{r},-} \rangle = \Delta_c \cos(\vec{Q}_c \vec{r} + \phi_c)$. At $\delta = 0.2$ we have to $M\vec{Q}_s = \vec{G}$ with $\vec{G}$ a reciprocal lattice vector and $M = 10$. The magnitude of the pinning decreases as a function of growing values of M and in the incommensurate case ($M \to \infty$) vanishes. To estimate the magnitude of the pinning, we solve the mean-field self-consistent equations for the moduli of the order parameters at fixed values of the phases. The mean-field energy then follows the form: $E^{HF} = E_0^{HF} + A_1 cos^2(\phi_1 + \pi/2) + A_2 cos^2(\phi_2)$ where $\phi_1 = 2\phi_c + \phi_s$ and $\phi_2 = -\phi_c + 2\phi_s$. For the $L_y = 8$ and $L_x = 30$ system at $\delta = 0.2$ we find that $A_1 \simeq -5 \times 10^{-5}$ while $A_2 \simeq 0.8t$. This implies that the pinning of the ϕ_1 mode is extremely small since it is proportional to $\sqrt{A_1}$. Following this point of view for the interpretation of the data, we will have to assume that the mass of the Φ_1 mode is beyond our numerical resolution so that we are not able to distinguish it from a genuine Goldstone mode. Pinning $\phi_2 = \pi/2$ and recalling that $\phi_1 = 2\phi_c + \phi_s$, and $2\vec{Q}_c = \vec{Q}_s$ locks together the dynamics of the spin and charge density wave. The QMC results of Fig. 4 support this point of view since the velocities of the spin and charge modes are comparable.

We have up till now concentrated on *narrow* rectangular lattices where the topology forces stripes to occur along only one direction. As the width of the system increases to approach a square topology, peaks in the structure factors are seen along both lattice directions. Fig. 5a,b plots the spin and charge structure factors for our largest system: $L_y = 12, L_x = 30$. The spin shows pronounced features not only at $(\pi - \epsilon_x, \pi)$ but also at $(\pi, \pi - \epsilon_y)$ where $\epsilon_x = \pi\delta$ and $\epsilon_y = 2\pi/L_y$. In the charge sector, cusps are seen at $(2\epsilon_x, 0)$ and $(0, 2\epsilon_y)$. There is however another feature namely a cusp at the wave vector (ϵ_x, ϵ_y) (Fig. 5b). For this lattice size the dynamical spin, $S_s(\vec{q}, \omega)$, and charge, $S_c(\vec{q}, \omega)$, structure factors are plotted in Fig. 5c,d. At the locations of peaks in the static structure factors soft modes in the dynamics are present.

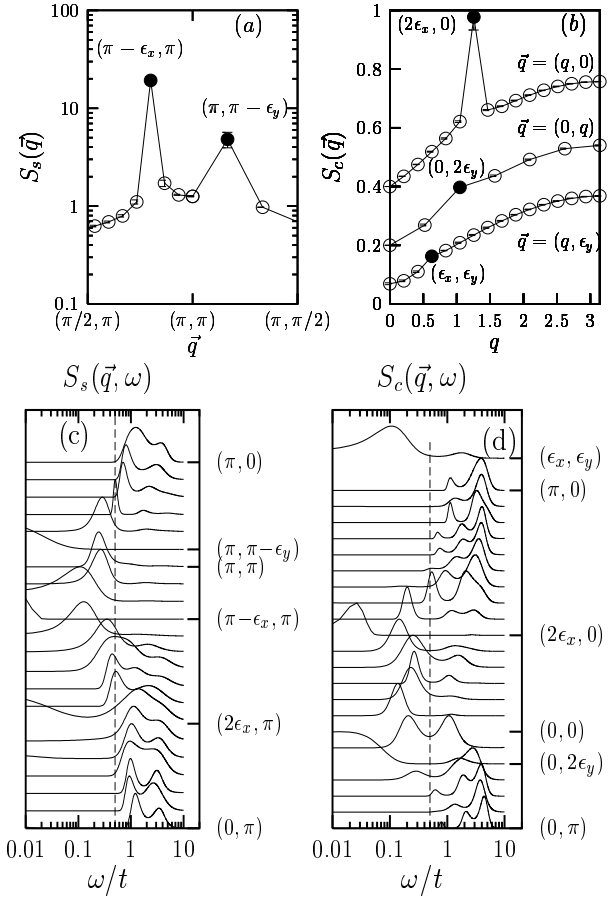

FIG. 5: Ground state spin and charge degrees of freedom on a 30×12 lattice $U/t = 3$, $\delta = 0.2$. (a), (b): static spin and charge structure factors. The bullets denotes $\vec{q}$ points where cusps or peaks are seen. (c),(d): dynamical spin and charge structure factor. The dashed line corresponds to twice the quasiparticle gap estimated from the density of states of Fig. 2c. For clarity we have normalized the data. The weight under each curve may be recovered from Fig. (a),(b) since $\int_0^\infty \mathrm{d}\omega S_{c/s}(\vec{q},\omega) = \pi S_{c/s}(\vec{q})$.

The lower edge of the spectra along the x-direction is plotted in Fig. 4. On this lattice topology, it is possible to arrange the holes in two stripes along the x-direction (corresponding to an incommensurate filling) or in five stripes along the y-direction. If the stripe ordering turns out to be long-ranged, one expects one of the two directions to be spontaneously chosen in the thermodynamic limit. On the other hand if there is no long-range stripe order, just short range fluctuations, we expect this state to remain stable as the size of the system grows. We note that a slave boson approach to the t-J model yields an identical pattern of spin and charge modes. For given soft spin modes at wave vectors $\vec{q} = (\pi \pm \epsilon, \pi \pm \epsilon)$ charge modes are generated at wave vectors $\vec{q} = (\pm 2\epsilon, \pm 2\epsilon)$ and $\vec{q} = (\pm\epsilon, \pm\epsilon)$ [12]. Our findings support this point of view.

To summarize, we have introduced a new QMC approach which allows us to obtain insight into doped Mott insulators. It is based on the observation that when the number of fermion flavors $N = 4n$, a broken spin-symmetry Hubbard model may be simulated with no sign problem regardless of the lattice topology and band filling. More generally, as a function of growing values of N the sign problem becomes less and less severe. Our approach clearly provides a way to go beyond Gaussian fluctuations around a given saddle point. On the other hand, it is at present not clear if the extrapolation from finite N to $N = 2$ is justified. We have used this method to investigate the doped Mott insulator at $N = 4$. We find a metallic state with no quasiparticles since there is a gap or pseudogap in the single particle density of states. The low energy excitations are collective spin and charge modes. On our largest rectangular topologies they are *gapless* in the spin sector at $(\pi \pm \epsilon_x, \pi)$ and $(\pi, \pi \pm \epsilon_y)$ and at $(\pm 2\epsilon_x, 0)$, $(0, \pm 2\epsilon_y)$, $(0, 0)$ as well $(\pm\epsilon_x, \pm\epsilon_y)$ in the charge sector.

We wish to thank the HLR-Stuttgart for generous allocation of computer time, the DFG for financial support (grant numbers AS 120/1-3 , AS 120/1-1) as well as a joint Franco-German cooperative grant (PROCOPE). FFA thanks P. Horsch and R. Zeyher for discussions.

[1] V. Emery, S. Kivelson, and J. Tranquada, Proc. Natl. Acad. Sci. USA **96**, 8814 (1999).
[2] H. Klauss, W. Wagener, M. Hillberg, W. Kopmann, H. Walf, F. Litterst, M. Hücker, and B. Büchner, Phys. Rev. Lett. **85**, 4590 (2000).
[3] F. F. Assaad, in *Lecture notes of the Winter School on Quantum Simulations of Complex Many-Body Systems :From Theory to Algorithms.*, edited by J. Grotendorst, D. Marx, and A. Muramatsu. (Publication Series of the John von Neumann Institute for Computing, 2002), Vol. NIC series Vol. 10., pp. 99–155.
[4] M. Jarrell and J. Gubernatis, Physics Reports **269**, 133 (1996).
[5] A. Auerbach, *Interacting electrons and quantum magnetism.*, *Graduate texts in contemporary physics* (Springer, New York, Berlin, Heidelberg, 1994).
[6] A. Parola, S. Sorella, M. Parrinello, and E. Tosatti, Phys. Rev. B **43**, 6190 (1991).
[7] H. Eskes, M. Mcinders, and G. A. Sawatzky, Phys. Rev. Lett. **67**, 1035 (1991).
[8] J. Voit, Rep. Prog. Phy. **57**, 977 (94).
[9] J. Zaanen, O. Osman, H. Kruis, Z. Nussinov, and J. Tworzydlo, Philos. Mag. B **81**, 1485 (2001).
[10] P. Lee, T. Rice, and P. Anderson, Solid State Commun. **14**, 703 (1974).
[11] G. Grüner, Rev. Mod. Phys. **66**, 1 (1994).
[12] P. Horsch and G. Khaliullin, unpublished .